Physica Medica 108 (2023) 102549

Contents lists available at ScienceDirect

Physica Medica

journal homepage: www.elsevier.com/locate/ejmp

Modeling of scavenging systems in water radiolysis with Geant4-DNA

Flore Chappuis [a], Veljko Grilj [a], Hoang Ngoc Tran [b], Sara A. Zein [b], François Bochud [a], Claude Bailat [a], Sébastien Incerti [b], Laurent Desorgher [a,*]

[a] Institute of Radiation Physics (IRA), Lausanne University Hospital and University of Lausanne, CH-1007 Lausanne, Switzerland
[b] Univ. Bordeaux, CNRS, LP2I Bordeaux, UMR 5797, F-33170 Gradignan, France

ARTICLE INFO

Keywords:
Water radiolysis
Scavenger
Geant4-DNA
FLASH effect

ABSTRACT

Purpose: This paper presents the capabilities of the Geant4-DNA Monte Carlo toolkit to simulate water radiolysis with scavengers using the step-by-step (SBS) or the independent reaction times (IRT) methods. It features two examples of application areas: (1) computing the escape yield of H_2O_2 following a ^{60}Co γ-irradiation and (2) computing the oxygen depletion in water irradiated with 1 MeV electrons.

Methods: To ease the implementation of the chemical stage in Geant4-DNA, we developed a user interface that helps define the chemical reactions and set the concentration of scavengers. The first application area example required two computational steps to perform water radiolysis using NO_2^- and NO_3^- as scavengers and a ^{60}Co irradiation. The oxygen depletion computation technique for the second application area example consisted of simulating track segments of 1 MeV electrons and determining the radio-induced loss and gain of oxygen molecules.

Results: The production of H_2O_2 under variable scavenging levels is consistent with the literature; the mean relative difference between the SBS and IRT methods is 7.2 % ± 0.5 %. For the oxygen depletion 1 μs post-irradiation, the mean relative difference between both methods is equal to 9.8 % ± 0.3 %. The results in the microsecond scale depend on the initial partial pressure of oxygen in water. In addition, the computed oxygen depletions agree well with the literature.

Conclusions: The Geant4-DNA toolkit makes it possible to simulate water radiolysis in the presence of scavengers. This feature offers perspectives in radiobiology, with the possibility of simulating cell-relevant scavenging mechanisms.

Introduction

Liquid water radiolysis is a major area of study from a fundamental point of view, especially regarding the structure of the radiation interaction pattern [1–4]. Understanding the effect of ionizing radiation on water also plays a role in diverse applications ranging from nuclear power technology to radiation biology [5,6]. Applied and fundamental research studies typically use aqueous solutions as samples. Monte Carlo (MC) simulations based on water-only irradiation are limited in this context. For example, MC simulations involving the irradiation of pure liquid water are not suitable for studying the production of radiolytic species in biologically relevant settings with, among others, the presence of oxygen molecules. With the renewed interest in radiation biology raised by the identification of the FLASH effect in radiotherapy [7], there is now a strong need to develop the publicly available Geant4-DNA track-structure simulation toolkit [8–11] for this application. The so-called FLASH effect refers to a biological differential effect induced by ultra-high dose rate irradiation and translates into both reduced toxicity to healthy tissues and equivalent tumor control with respect to conventional dose rate irradiation. In radiation chemistry, the use of solutes in water has made it possible to investigate the inhomogeneous kinetics of radio-induced species as well as determine radiation chemical yields and reaction mechanisms [12,13]. The possibility of simulating the conditions of these experiments with Geant4-DNA is relevant to this field as well.

Whether studying the impact of oxygen or various solutes in water radiolysis, the same simulation strategy applies: adding the chemical effect of homogeneously distributed molecules, also termed scavengers, into the simulation process. Adding these molecules disturbs the radiolysis mechanism by introducing competing chemical reactions that are

* Corresponding author at: Institute of Radiation Physics (IRA), Rue du Grand-Pré 1, 1007 Lausanne, Switzerland.
E-mail address: laurent.desorgher@chuv.ch (L. Desorgher).

https://doi.org/10.1016/j.ejmp.2023.102549
Received 5 October 2022; Received in revised form 11 January 2023; Accepted 13 February 2023
Available online 13 March 2023

meant, for some applications, to control the production of targeted radio-induced species. This competition takes place during the chemical stage of water radiolysis, which is one of the three stages implemented in Geant4-DNA. Briefly, the three stages of the Geant4-DNA simulation scheme are: the physical, physico-chemical, and chemical. After excitation and ionization of water molecules during the physical stage, different processes generate radiolytic species in the physico-chemical stage [10]. These species diffuse and react with each other during the initially inhomogeneous chemical stage. The effect of scavengers occurs during this latter stage, which Geant4-DNA can simulate either using the step-by-step (SBS) method or the independent reaction times (IRT) method [14]. Both methods model the Brownian motion of species and the reaction mechanism. With the SBS method, the trajectory of species is calculated on a step-by-step diffusion basis – which is resource intensive – and two species react when their separation distance is below a given threshold. The IRT method, on the other hand, calculates random times of reaction from the initial position of species. This approach provides a higher computational efficiency than the SBS method to model the diffusion–reaction mechanism but suffers from the loss of information on the position of radiolytic species over time. Geant4-DNA lacks a comprehensive structure for the use of scavengers in the two methods available for the chemical stage of radiolysis. Our study aimed to develop this aspect of the toolkit. The ability to simulate the presence of scavengers in water radiolysis is also available with other MC track-structure codes such as PARTRAC [15], RITRACKS [14], TRAX-CHEM [16], IONLYS-IRT [17], TOPAS-nBio [18], and gMicroMC [19].

In this work, we implemented the scavenger model in the SBS method of Geant4-DNA. The model was already available for the IRT method since Geant4 version 10.7 [20], but we developed a user-friendly interface to ease its use. To validate the scavenger model and compare the two methods, we computed the following quantities in different scavenging conditions: (1) the escape yield of hydrogen peroxide (H_2O_2) following a ^{60}Co γ-irradiation and (2) the oxygen (O_2) depletion in liquid water irradiated with 1 MeV electrons. The former is an application coming from radiochemistry where the scavenging system is a combination of nitrite (NO_2^-) and nitrate (NO_3^-) ions at different concentrations; the computed yields are validated against experimental data from the literature. The latter is closer to situations encountered in radiobiology: the scavenger is the oxygen molecule added to water in a variety of partial pressures; the results are compared with the literature and experimental measurements obtained using the Oriatron eRT6 electron linac [21]. Determining the oxygen depletion caused by an irradiation is of particular interest in the search for the mechanism of the FLASH effect. The oxygen depletion hypothesis [22], one of the mechanisms proposed in the literature, builds on the difference in duration between a conventional (CONV) and ultra-high dose rate (UHDR) irradiation. According to this hypothesis, at UHDR, the time delay to re-oxygenate normal tissues causes a transient radio-induced hypoxia in these tissues that lowers their radiosensitivity and spares them from the deleterious effect of radiation. We will discuss this hypothesis in light of the current state of research.

Materials and methods

Scavenger model in the pure liquid water radiolysis

The model developed in Geant4-DNA does not treat scavengers from a particle-based approach but as a continuum [23]. This continuum approximation considers the scavenger particles to be homogeneously distributed in water. In Geant4-DNA, their effects are introduced in the chemical stage of the water radiolysis process by defining the scavenger-specific chemical reactions and the concentration of scavengers. We disregard the physical interaction of radiation with the scavenger – which would occur during the physical stage of the Geant4-DNA simulation scheme – as the concentration of scavengers should be sufficiently low (below 1 M [14]). On the other hand, the number of such molecules is considered large enough to assume no variation in concentration during the chemical stage of the simulation.

The differential equation (1) describes the reaction of a radio-induced species X with a scavenger S

$$\frac{d[X]}{dt} = -k\,[S]\,[X], \tag{1}$$

where k is the reaction rate ($M^{-1}s^{-1}$) and the square brackets indicate a concentration in molar. As the concentration of the scavenger remains constant over time, this reaction behaves like a first-order reaction whose solution is an exponentially decaying function. The probability of a reaction between X and S during the time step Δt is therefore given by equation (2):

$$1 - e^{-k[S]\,\Delta t}. \tag{2}$$

The reader can refer to Ramos-Méndez et al. [20] for the description and the implementation in Geant4-DNA of the scavenger model with the IRT method. For the SBS method, we have included an additional process for species – named "DNAScavenger" – in the G4EmDNAChemistry constructor. This process determines the probability of reaction with the scavenger and transfers this probability into a reaction time to generate a time step. In particular, it generates the following time step from reaction data (scavenger concentration and reaction rate):

$$\Delta t = \frac{-\ln(U)}{k\,[S]}, \tag{3}$$

where U is a random number uniformly generated over $]0,1[$. The algorithm chooses the smallest step proposed by all processes associated with the species and continues the simulation on this step-by-step basis. The $-\ln(U)$ parameter is re-evaluated at each step using the previous one: see the Geant4 Physics Reference Manual [24] for more details.

User interface for the chemical stage of Geant4-DNA

The chemical reaction table is an input for the Geant4-DNA chemical stage, which the user can freely modify. To ease the addition/removal of any chemical reaction from this table, we developed a user interface which consists of a text file (Fig. 1). This interface allows handling chemical reactions, their associated reaction rates, and the concentration of scavengers. For the IRT method, the type assigned to each chemical reaction specifies how the reaction will be treated among the following options [25]: fully or partially diffusion-controlled reactions with or without Coulombic force for types 1 to 4; consideration of the spin effect for type 5 reactions; first-order reactions (decay of species) or pseudo-first-order reactions (reactions with a scavenger) for type 6. The SBS method does not yet include these different reaction types. Chemical reactions are either fully diffusion-controlled or of type 6.

The interface was released as an example in Geant4 version 11.0 (examples/extended/medical/dna/scavenger) and is currently only publicly available for the IRT method. The example provides two reaction tables: one with the NO_2^-/NO_3^- system and the other with oxygen as a scavenger (Fig. 1). In addition to scavenger-specific reactions, the tables include a restricted number of radio-induced chemical reactions. The users can extend this list according to their application needs.

Radiolytic H_2O_2 production and scavengers (NO_2^-/NO_3^-)

Water radiolysis generates H_2O_2 molecules mainly through the reaction of two $^{\bullet}$OH radicals (Equation (4a) [26]). In the early chemical stage, other radiolytic species such as solvated electrons (e_{aq}^-) diffuse throughout the volume. Solvated electrons efficiently react with freshly produced H_2O_2 molecules and constitute the main factor of H_2O_2 loss (Equation (4b) [26]). The presence of specific scavengers can artificially modify this mechanism: scavengers directed towards $^{\bullet}$OH reduce the

```
# Definition of scavengers ---------------
# scavenger: NAME  CONCENTRATION [mole/l]
#----------------------------------------
scavenger: O2   5.20e-05  # 4% in partial pressure

# Reactions between radio-induced species --------------------
# REACTANTS -> PRODUCTS , RATE [1/s/(mole/l)] or [1/s]   TYPE
#-----------------------------------------------------------
e_aq + e_aq + [H2O] + [H2O] -> H2 + OH- + OH- , 6.36e9      type_3
e_aq + OH -> OH- ,                              2.95e10     type_2
e_aq + H + [H2O] -> H2 + OH- ,                  2.50e10     type_1
e_aq + H3O+ -> H + [H2O] ,                      2.11e10     type_4
e_aq + H2O2 -> OH- + OH ,                       1.10e10     type_2
OH + OH -> H2O2 ,                               5.50e9      type_2
OH + H -> [H2O] ,                               1.55e10     type_2
H + H -> H2 ,                                   5.03e9      type_1
H3O+ + OH- -> [H2O] + [H2O] ,                   1.13e11     type_3

# Reactions with the scavengers
# Specify the scavenger with []
#------------------------------
e_aq + [O2] -> O2- , 1.74e10    type_6
H + [O2] -> HO2 ,    2.10e10    type_6
O- + [O2] -> O3- ,   3.70e9     type_6
```

Fig. 1. User interface to define chemical reactions and the concentration of scavengers in the Geant4-DNA chemical stage. This example uses the IRT method and is available in the Geant4 extended examples: examples/extended/medical/dna/scavenger (release 11.0). In addition to the nine elemental chemical reactions listed, the user can add other reactions as long as each molecular species is defined in the C++ code. Users can specify reactions with scavengers in the interface by surrounding the name of the scavenger with square brackets. Each chemical reaction has a type assigned to it (from 1 to 6) according to Frongillo et al. [25].

production of H_2O_2, and the e^-_{aq} scavengers prevent it from reacting with H_2O_2.

$$^{\bullet}OH + {}^{\bullet}OH \rightarrow H_2O_2 \qquad k_{4a} = 5.5{\cdot}10^{9}\ M^{-1}s^{-1} \tag{4a}$$

$$H_2O_2 + e^-_{aq} \rightarrow OH^- + {}^{\bullet}OH \qquad k_{4b} = 1.1{\cdot}10^{10}\ M^{-1}s^{-1} \tag{4b}$$

In this work, we used NO_2^- as an $^{\bullet}OH$ scavenger and NO_3^- to scavenge e^-_{aq}. In addition to reacting with $^{\bullet}OH$ radicals, NO_2^- also scavenges e^-_{aq}, although less efficiently than NO_3^-. Equations (5a), (5b), and (5c) [26] summarize the effect of the NO_2^-/NO_3^- scavenging system on water radiolysis as we implemented it in the chemical stage of Geant4-DNA.

$$^{\bullet}OH + NO_2^- \rightarrow {}^{\bullet}NO_2 + OH^- \qquad k_{5a} = 1.0{\cdot}10^{10}\ M^{-1}s^{-1} \tag{5a}$$

$$e^-_{aq} + NO_2^- \rightarrow {}^{\bullet}NO_2^{2-} \qquad k_{5b} = 4.1{\cdot}10^{9}\ M^{-1}s^{-1} \tag{5b}$$

$$e^-_{aq} + NO_3^- \rightarrow {}^{\bullet}NO_3^{2-} \qquad k_{5c} = 9.7{\cdot}10^{9}\ M^{-1}s^{-1} \tag{5c}$$

We selected NO_2^- for the simulation instead of other $^{\bullet}OH$ radical scavengers (e.g. C_2H_5OH, CH_3OH, Br^-) because of its high reactivity towards $^{\bullet}OH$. This feature limits the concentration of NO_2^- (compared to less reactive scavengers) to achieve the highest scavenging capacities – scavenging capacity being the multiplication of the reaction rate by the scavenger concentration. In order to reach the maximum scavenging capacity used ($10^{10}\ s^{-1}$), the required concentration is 1 M with the NO_2^- ions. Adding scavenger concentrations above 1 M would induce systematic errors, since the modeling does not account for the direct interaction of ionizing radiation with scavengers. The bromide anion (Br^-) strongly reacts with $^{\bullet}OH$ radicals as well, but involves a complicated reaction scheme [27]. We therefore preferred NO_2^- over Br^-.

Simulating H_2O_2 formation by ^{60}Co γ-irradiation in the presence of scavengers

To simulate a ^{60}Co irradiation modality and the subsequent

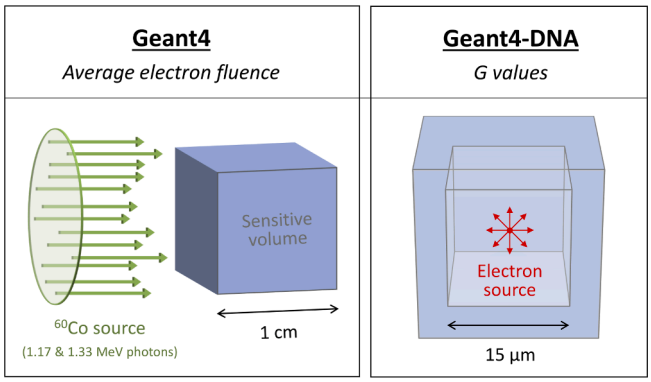

Fig. 2. Procedure for simulating water radiolysis by a ^{60}Co source: schematic of the Geant4 simulation (left) and geometry for the Geant4-DNA simulation (right).

radiolysis with scavengers, we performed two computational steps: (a) using Geant4 [28–30] to determine the spectral distribution of the average electron fluence within a pure water sample irradiated with a ^{60}Co source and (b) using Geant4-DNA to simulate radiolysis with scavengers (NO_2^- and NO_3^-), the irradiation source being electrons whose spectral distribution is generated from the average electron fluence of step (a).

Based on the theorem by A. M. Kellerer [31], the average electron fluence $\overline{\Phi}$ within a volume results from the sum of the electron track lengths divided by the computational volume. The spectral distribution of the average electron fluence is obtained by discretizing the average fluence into energy bins (for a detailed explanation of the method, see section 3.2 Method II of Hartmann and Andreo [32]). To derive the electron tracks generated by the interaction of ^{60}Co photons with water, we used the general purpose Geant4 toolkit (release 11.0). The geometry of the MC simulation consisted of a $1 \times 1 \times 1\ cm^3$ water cube, irradiated with a uniform monodirectional field of photons perpendicular to one side of the cube (see Fig. 2); the field contained an equal number of 1.173 MeV and 1.332 MeV γ-rays (pertaining to the two ^{60}Co spectrum peaks). The electron tracks were scored within the water cube and their contribution grouped into energy bins ranging from 1 keV to 1.5 MeV, with a logarithmic scale of 150 bins.

The primary source for the radiolysis simulations with Geant4-DNA (release 11.0) was an isotropic point-like electron source, whose spectrum was obtained by the previous Geant4 simulation (Fig. 2). This source was placed in the center of a $1 \times 1 \times 1\ km^3$ volume filled with water containing a variable concentration of NO_2^- and 25 mM NO_3^-. This large volume ensures the free diffusion of radiolytic species. The concentration of NO_2^- varied from 10 µM to 1 M to cover a wide range of $^{\bullet}OH$ scavenging level. The physical stage of the simulation was limited by a $15 \times 15 \times 15\ \mu m^3$ virtual box centered on the source, that is all particle tracks (primaries and secondaries) were killed when reaching the surface of this box. The virtual box dimension ensured that the volume was large enough to simulate a sufficient number of physical interactions, but not excessively large to avoid an over-contribution of low energy electrons. In this geometry, the larger volume of $1 \times 1 \times 1\ km^3$ (considered an infinite volume at the scale of the simulation) enabled the positioning and diffusion of the radiolytic species produced in the vicinity of the surface of the virtual box during the physico-chemical and chemical stages of Geant4-DNA. The list of chemical reactions for this application is available in Tables S1 and S2 of the Supporting Materials.

Oxygen depletion: Simulation setup

Using the Geant4-DNA toolkit (release 11.0), we computed the ox-

ygen depletion induced by 1 MeV electrons (upper energy limit of the Geant4-DNA models) at initial partial pressures of oxygen ranging from 0 % atm to 21 % atm[a] and three different durations of the radiolysis process: 1 μs, 2 μs, and 1 ms. The partial pressures pO_2 [atm] convert to concentration c [M] of dissolved oxygen according to Henry's law: $c = 1.3{\cdot}10^{-3}{\cdot}pO_2$, at 25 °C [33]. The computation for both SBS and IRT methods involved independent electrons of 1 MeV (initial kinetic energy), simulated until they lose between 10 keV and 10.1 keV of energy [34]. This procedure is typical of track-structure codes, where the scoring of radiolytic species is restricted to electron track segments. The obtained radiolytic yields thus refer to the initial kinetic energy of the primary electron: 1 MeV in this case, which is a good approximation of the nominal energy of the eRT6 beam (between 5 MeV and 6 MeV) in terms of effects on water radiolysis since the collisional stopping power is approximately constant in this energy range. For each electron track, the code scored the loss and gain of oxygen molecules during the simulation. The resulting oxygen depletion for the different independent electrons was then averaged to obtain the mean oxygen depletion and associated track-segment G value $G(-O_2)$, which is the ratio between the mean oxygen depletion and the mean sum of energy deposits $\overline{E}_{dep}$ [eV]:

$$G(-O_2) = \frac{\overline{N(-O_2) - N(+O_2)}}{\overline{E}_{dep}} \cdot 100, \tag{6}$$

where $N(\pm O_2)$ is the number of oxygen molecules lost (−) or gained (+) during the chemical stage of the simulation. The computed depletion G values in units of $(100\ eV)^{-1}$ are finally converted into a percentage (partial pressure) per 10 Gy, for direct comparison with experimental data. With this methodology, the electron tracks are regarded as independent, which corresponds to a conventional dose rate irradiation. Indeed, consider as an example a 10 Gy electron irradiation at 0.1 Gy/s. For minimum ionizing electrons, the fluence is ~ 312 μm^{-2}[b], and the average time interval between two consecutive electrons on 1 μm^2 is therefore ~ 321 ms. This duration is long enough for the radiolytic species to have diffused and reacted; the probability for inter-track interaction of radiolytic species is negligible. The list of chemical reactions for this application is available in Tables S1 and S3 of the Supporting Materials.

Oxygen depletion: Experimental measurements

We used the OxyLite™ Pro (Oxford Optronix ltd., Abingdon, United Kingdom) dissolved oxygen and temperature monitor to evaluate in real time the change of oxygen partial pressure in Milli-Q® (Merck SA, Darmstadt, Germany) water under electron irradiation. The Oriatron eRT6 [21], a 6 MV electron linac, served as a source of energetic electrons delivering a dose rate of 0.1 Gy/s at the target position. Numerous samples pre-equilibrated to pO_2 between 0 % atm and 20 % atm were exposed to single doses of 10 Gy or 20 Gy in several experiments carried out during almost a one-year period. The depletion rate was calculated by dividing the difference in average pO_2 value (30 s average) before and after irradiation by the delivered dose. More details are available in the Supporting Materials.

Results

Influence of scavengers on H_2O_2 formation by ^{60}Co γ-irradiation

This section is divided into two parts reporting the two computational steps to simulate radiolysis using a ^{60}Co irradiation modality: The first subsection presents the spectral distribution of the average electron fluence within a 1 × 1 × 1 cm^3 water sample irradiated with a ^{60}Co source; The second subsection covers the radiolysis simulation to compute the G values of H_2O_2 in different scavenging systems.

Average electron fluence in water irradiated with a ^{60}Co source

Fig. 3 shows the average electron fluence within a 1 × 1 × 1 cm^3 water volume irradiated with an equal number of 1.173 MeV and 1.332 MeV photons (^{60}Co source). This distribution computed with the Geant4 toolkit makes it possible to specify the primary particle energies for the Geant4-DNA simulation.

H_2O_2 in water radiolysis with scavengers

Fig. 4A shows the computed G values of H_2O_2 (green and red filled markers) at 10 μs after irradiation with a ^{60}Co source for concentrations of NO_2^- ranging from 10 μM to 1 M, the concentration of NO_3^- being fixed at 25 mM. The figure also shows the experimental data [35–38] (black empty markers) available in the literature with 25 mM of NO_3^- and different $^{\bullet}OH$ radical scavengers: ethanol (C_2H_5OH), methanol (CH_3OH), and bromide (Br^-). To compare the NO_2^-/NO_3^- system with the other scavenging systems used in the literature, the results are presented as a function of the $^{\bullet}OH$ radical scavenging capacity, in other words the concentration of the $^{\bullet}OH$ scavenger times the reaction rate. Equations (7a), (7b), (7c), and (7d) give the scavenging reactions and associated reaction rates [26] to calculate the scavenging capacities (with respect to $^{\bullet}OH$) of each solute. The inset Fig. 4B presents the temporal evolution of the computed G values for different levels of $^{\bullet}OH$ radical scavenging.

$$^{\bullet}OH + NO_2^- \rightarrow {}^{\bullet}NO_2 + OH^- \qquad k_{7a} = 1.0{\cdot}10^{10}\ M^{-1}s^{-1} \tag{7a}$$

$$^{\bullet}OH + C_2H_5OH \rightarrow CH_3C^{\bullet}HOH + H_2O \qquad k_{7b} = 1.9{\cdot}10^{9}\ M^{-1}s^{-1} \tag{7b}$$

$$^{\bullet}OH + CH_3OH \rightarrow {}^{\bullet}CH_2OH + H_2O \qquad k_{7c} = 9.7{\cdot}10^{8}\ M^{-1}s^{-1} \tag{7c}$$

$$^{\bullet}OH + Br^- \rightarrow BrOH^{\bullet -} \qquad k_{7d} = 1.1{\cdot}10^{10}\ M^{-1}s^{-1} \tag{7d}$$

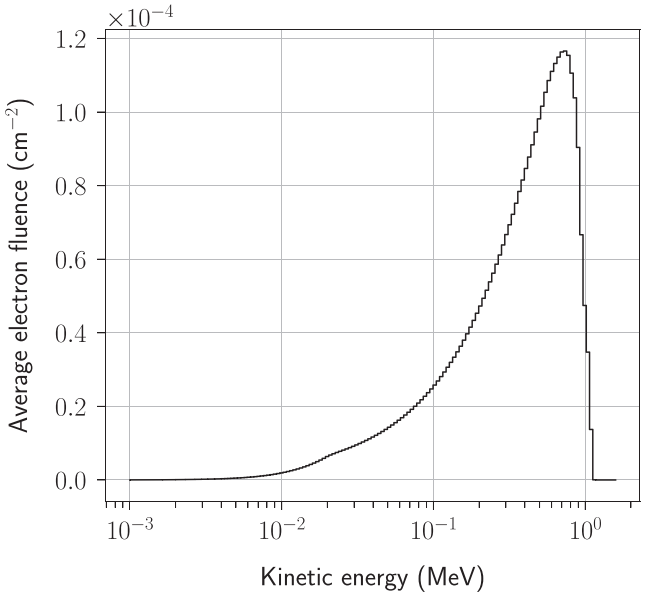

Fig. 3. Average electron fluence within a 1 × 1 × 1 cm^3 water cube γ-irradiated with a ^{60}Co source consisting of an equal number of 1.173 MeV and 1.332 MeV photons; the fluence was normalized by the number of simulated primary photons. This distribution corresponds to $d\overline{\Phi}/dE$ multiplied by the width of the energy bins. The statistical uncertainty for each bin is within 1 %.

[a] percentage of sea-level pressure.

[b] fluence = dose/mass_stopping_power, with mass_stopping_power = 2 MeV cm^2/g.

Oxygen depletion: Simulation

Fig. 5 gathers the computed oxygen depletion G values after a 1 MeV electron irradiation for various initial partial pressures of oxygen. In particular, Fig. 5A shows the results of both Geant4-DNA simulation methods – the IRT method and the SBS method – 1 μs after the start of the radiolysis process. For the SBS and IRT methods, the radio-induced oxygen depletions at $pO_2 = 21$ % atm amount to 0.29 % atm / 10 Gy and 0.26 % atm / 10 Gy, respectively. To investigate the temporal evolution of the depletion, we extended the computation with the IRT method to 2 μs and 1 ms post-irradiation and present the results in Fig. 5B.

Oxygen depletion: Experimental measurements

Fig. 6 shows the measured oxygen depletion data collected over almost a year using the OxyLite™ Pro monitor and the Oriatron eRT6 electron linac as the irradiation modality. We pooled all these experiments together and calculated the mean – 0.23 % atm / 10 Gy – and standard deviation – 0.01 % atm / 10 Gy – of the data set. The standard deviation quantifies the spread of the measured values. In the absence of precise knowledge about the variability of individual measurement uncertainties, we use the standard deviation as an estimator of uncertainty.

Discussion

Influence of scavengers on H_2O_2 formation by ^{60}Co γ-irradiation

The NO_2^-/NO_3^- scavenging system introduces competing reactions, thus artificially influencing the water radiolysis mechanism. Fig. 4A presents the result of this influence on the production of stable and experimentally detectable H_2O_2 molecules. It shows that the competition caused by the chemical system depends on the amount of scavengers in water: increasing the concentration of NO_2^- reduces the number of H_2O_2 produced. The simulations (with either the SBS method or the IRT method) agree with the literature [35–38]. Both methods follow the expected scavenging behavior, therefore validating the computation method for the scavenging process in Geant4-DNA. Also, the two methods closely agree with a mean relative difference of 7.2 % ± 0.5 %. The SBS and IRT methods model the diffusion–reaction mechanism differently, however, the classification of chemical reactions into six types for the IRT method is a major difference from the SBS method, which does not yet include this specificity. It is also worth noting that the chemical evolution of the system directly depends on the physical stage of the simulation [34]. The initial spatial distribution of radiolytic species, which is provided by the track interaction pattern, has obvious consequences on the G values of H_2O_2. Future improvements in the physical models of Geant4-DNA, especially for low energy electrons (below a few hundred eV), may significantly influence the radiolysis outputs [39–41,10].

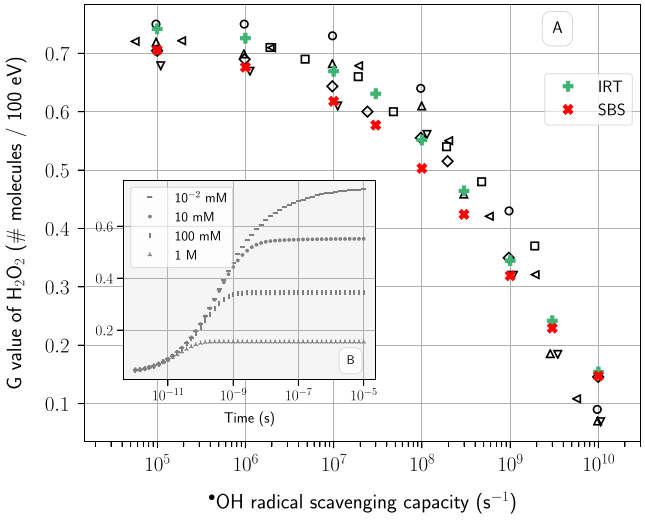

Fig. 4. Impact of scavengers on the production of H_2O_2 after a ^{60}Co γ-irradiation. (A) G values of H_2O_2 as a function of the scavenging capacity for •OH radicals: (✚) NO_2^- and 25 mM NO_3^- with the IRT method, this work; (✖) NO_2^- and 25 mM NO_3^- with the SBS method, this work; (□) C_2H_5OH and 25 mM NO_3^- [35]; (○) CH_3OH and 25 mM NO_3^- [36]; (◇) CH_3OH and 25 mM NO_3^- [37]; (△) CH_3OH and 25 mM NO_3^- [38]; (▽) Br^- and 25 mM NO_3^- [38]; (◁) C_2H_5OH and 25 mM NO_3^- [38]. (B) Evolution over time of the G values of H_2O_2 at selected concentrations of NO_2^- and 25 mM NO_3^- with the IRT method, this work. The statistical uncertainty of the simulations is below 1 %.

To better understand the impact of the NO_2^-/NO_3^- system, Fig. 4B shows how H_2O_2 evolves over time for various concentrations of NO_2^-. The amount of H_2O_2 converges to a different G value depending on the scavenger concentration. The multiplication of this concentration with the rate constant for the scavenging reaction ($1.0 \cdot 10^{10}$ $M^{-1}s^{-1}$) gives the scavenging capacity associated with the G value of H_2O_2, and the link to Fig. 4A. The scavenger concentration is therefore directly proportional to the scavenging capacity, which in turn is inversely proportional to the scavenging time. Knowing the concentration of NO_2^- makes it possible to predict the •OH scavenging time: 100 mM NO_2^- highly impact H_2O_2 production at around 1 ns post-irradiation (10^{-10} M s·10 M^{-1} $= 10^{-9}$ s). The effective time scale at which scavengers affect the system thus depends on their concentration, but also on their reactivity.

Simulating the ^{60}Co γ-irradiation and the subsequent radiolysis was a two-step procedure (Fig. 2). In particular, the geometry of the Geant4-DNA simulation includes a virtual box of 15 × 15 × 15 μm^3, which restricts the physical stage of the water radiolysis process in space. We chose the virtual box dimension based on two main concerns: a large enough volume to limit possible artifacts caused by a lack of physical interactions inside the virtual box but a small enough volume to avoid over-contribution of low energy electrons. Indeed, the energy of the primary source particles is randomly sampled from the average electron fluence distribution (Fig. 3). If an electron loses a large amount of energy, its contribution to the G value of H_2O_2 may include the contribution of a lower energy primary electron generated from the same energy distribution of Fig. 3. This problem mainly affects the lower side of the distribution since electrons above ~ 300 keV have approximately the same collisional stopping power [42] and then provide similar G values of H_2O_2. For example, consider a 60 keV electron whose stopping power in liquid water equals ~ 6 MeV/cm [42]. For a 10 × 10 × 10 μm^3 virtual box, the shortest travelling distance of the electron would be 5 μm (assumption of a straight track), which corresponds to 3 keV of lost energy. In a 20 × 20 × 20 μm^3 virtual box, the electron would lose at least 6 keV. The latter case shows that the loss of energy becomes large, which implies a change in the structure of the track interaction pattern. The contribution of this 60 keV electron to the G value of H_2O_2 would also include the contribution of a lower energy electron in this case. To determine the effective impact of a change in the virtual box dimension, we computed G values of H_2O_2 in the same conditions as presented in the materials and methods section but with smaller or larger virtual boxes. Taking the virtual box of 15 × 15 × 15 μm^3 as the reference, the mean relative differences in the G values of H_2O_2 for different virtual boxes are: − 16.6 % ± 0.2 % for a 5 × 5 × 5 μm^3 virtual box, − 5.2 % ± 0.2 % for a 10 × 10 × 10 μm^3 virtual box, 3.1 % ± 0.2 % for a 20 × 20 × 20 μm^3 virtual box, and 7.1 % ± 0.2 % for a 30 × 30 × 30 μm^3 virtual box. The difference between the successive mean relative differences gradually decreases as the dimension of the virtual box increases, indicating that the artifacts caused by a lack of physical interactions inside the virtual box (small virtual box dimensions) have a greater impact than an over-contribution of low energy electrons due to large virtual box dimensions.

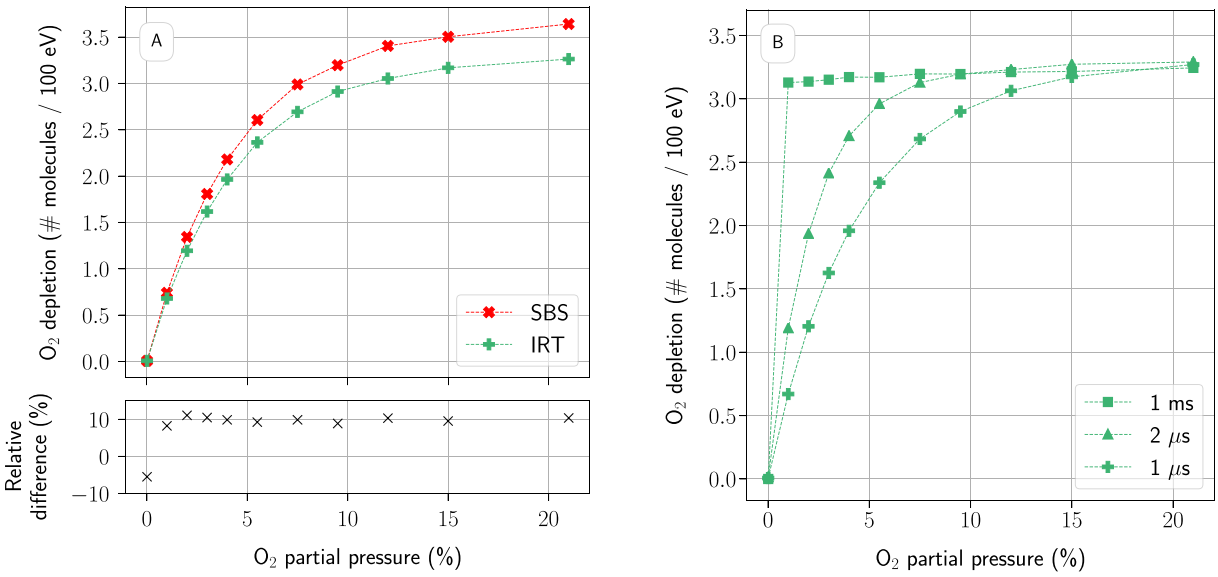

Fig. 5. Computed depletion G values of diluted oxygen for different water oxygenation levels. (A) Comparison between the SBS and IRT methods of Geant4-DNA at 1 μs post-irradiation. (B) Oxygen depletion G values at three different time points following irradiation (IRT method). These results combine independent track segments of 1 MeV electrons with energy loss in the range [10 keV, 10.1 keV]. The statistical uncertainty of the simulations is below 1 %.

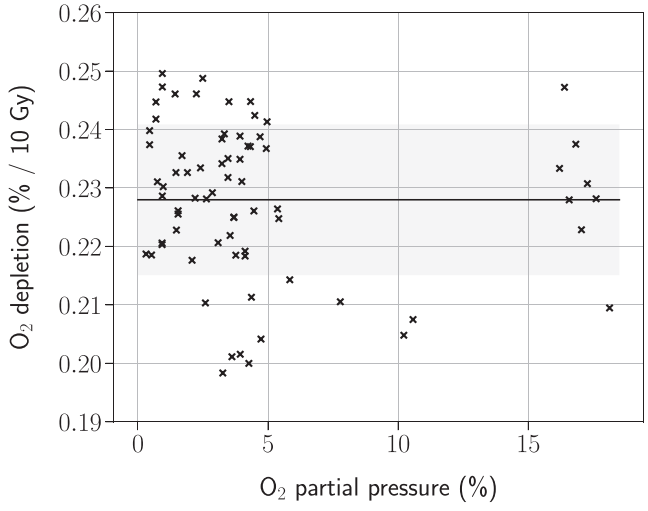

Fig. 6. Oxygen depletion rate measured in Milli-Q® water (data set obtained with single 10 Gy or 20 Gy irradiations). The horizontal black line indicates the mean of the data set (0.23 % atm / 10 Gy) and the shaded area shows measurements within one standard deviation (0.01 % atm / 10 Gy).

Oxygen depletion

The oxygen molecule is an important element in biological tissues and probably plays a role in the mechanism responsible for the FLASH effect. In water radiolysis, this molecule acts as a scavenger – mainly of e^-_{aq} – but in the context of the oxygen depletion hypothesis [22], the radiolytic oxygen depletion is the relevant indicator. In Fig. 5B, the evolution of oxygen depletion with increasing time after irradiation indicates that the depletion rate does not depend on the initial partial pressure of oxygen. When the amount of oxygen is low, the radiolytic species (e^-_{aq}, $H^\bullet$, $O^{\bullet-}$) need more time to reach and react with an oxygen molecule. At 1 μs post-irradiation, the amount of depleted oxygen is therefore pO_2-dependent. This dependence slowly disappears as soon as the observation time increases. However, it should be noted that the simulation technique has limitations. Due to computing time and memory issues, the scoring of radiolytic species is restricted to electron track segments in an infinitely large volume. Beyond the microsecond scale, the radio-induced species continue to freely diffuse, without encountering species from another track for example. In this configuration, the radio-induced species move away from each other, thus gradually decreasing the probability of mutual reaction. The simulation procedure is valid for the inhomogeneous chemical stage of water radiolysis, therefore, the results at 1 ms post-irradiation constitute a theoretical extrapolation. One possibility to overcome this limitation would be to use a compartment-based model as presented by Tran et al. [43]. This approach is especially dedicated to the modeling of water radiolysis beyond the inhomogeneous chemical stage.

For the oxygen depletion at 1 μs post-irradiation (Fig. 5A), the mean relative difference between the SBS and IRT methods is equal to 9.8 % ± 0.3 % (contribution at $pO_2 = 0.01$ % atm excluded). Based on the three chemical reactions – Equations (8a), (8b), and (8c) [14] – that consume oxygen in the model, the contribution of each to the mean relative difference is as follows: the chemical reaction (8a) causes the largest contribution (4.6 % ± 0.2 %); the second contribution comes from reaction (8b) with 4.2 % ± 0.1 %; the last chemical reaction (8c) weakly impacts the mean relative difference (0.24 % ± 0.02 %) since the production of $O^{\bullet-}$ is very low (no more than 0.1 molecule per 100 eV).

$$e^-_{aq} + O_2 \rightarrow O_2^{\bullet-} \qquad k_{8a} = 1.74{\cdot}10^{10}\ M^{-1}s^{-1} \tag{8a}$$

$$H^\bullet + O_2 \rightarrow HO_2^\bullet \qquad k_{8b} = 2.1{\cdot}10^{10}\ M^{-1}s^{-1} \tag{8b}$$

$$O^{\bullet-} + O_2 \rightarrow O_3^{\bullet-} \qquad k_{8c} = 3.7{\cdot}10^{9}\ M^{-1}s^{-1} \tag{8c}$$

At $pO_2 = 21$ % atm, the radio-induced oxygen depletions amount to 0.29 % atm / 10 Gy and 0.26 % atm / 10 Gy for the SBS method and the IRT method, respectively. These results are consistent with the experimental measurement presented in this work – 0.23 % atm ± 0.01 % atm / 10 Gy – and the literature: for example, Boscolo et al. [44] computed a depletion of 0.26 % atm / 10 Gy for 1 MeV electrons. Table 1 presents several other oxygen depletions reported in the literature. Lai et al. [19] obtained lower depletion rates in a different simulation setup and observed a dependence on the instantaneous dose rate. The study by Weiss et al. [45] reports that oxygen depletion depends on the type of irradiated cells. In water samples irradiated at different dose rates and with three radiation modalities, Jansen et al. [46] observed a dose rate dependency of oxygen depletion: it decreases with increasing dose rates.

Table 1
Computed and measured oxygen depletion rate in different media and irradiation conditions.

Model	Radiation source	Oxygen depletion (% atm / 10 Gy)[a]	Reference
Geant4-DNA Monte Carlo code	1 MeV electrons	0.29, 0.26	this work
TRAX-CHEM Monte Carlo code	1 MeV electrons	0.26	[44]
gMicroMC Monte Carlo code	4.5 keV electrons	0.15 – 0.18	[19]
Water	6 MV electrons	0.23 ± 0.01	this work
	225 kV X-rays	0.04 – 0.18	
	224 MeV protons	0.04 – 0.25	[46]
	carbon ions	0.09 – 0.17	
Phosphate-buffered saline solution with 5 % BSA[b]	10 MeV electrons – 0.1 Gy/s	0.25, 0.28	[47]
	10 MeV electrons – 300 Gy/s	0.22 ± 0.01	
α medium (cell culture)	25 MV X-rays	0.34 ± 0.04	[48]
α medium (cell culture) with serum	^{60}Co	0.43 ± 0.05	[49]
	270 kVp X-rays	0.35	[50]
E. coli B/r bacterial suspension	^{60}Co	0.45 ± 0.08	[45]
Nude mice, normal tissue	10 MeV electrons – 270 Gy/s	0.15 ± 0.02	[47]
Nude mice, tumor tissue		0.07 ± 0.01	

[a] conversion factor for depletion rates published in [M/(dose unit)]: $1.3 \cdot 10^{-3}$ M/atm (Henry's constant at 25 °C).
[b] bovine serum albumin.

Their results vary from 0.04 % atm to 0.18 % atm / 10 Gy for 225 kV X-rays, 0.04 % atm to 0.25 % atm / 10 Gy for 224 MeV protons, and 0.09 % atm to 0.17 % atm / 10 Gy for carbon ions.

The oxygen depletion, whether computed or measured, is low for standard doses of FLASH radiotherapy treatment (10 Gy to 30 Gy) [7]. Researchers reported different depletion measurements in various conditions ranging from pure water to mice. The variability of these results reveals the dependence of oxygen depletion on experimental conditions (in vitro/in vivo, dose rates, cell types, irradiation modalities). On the other hand, water radiolysis simulations are able to determine oxygen depletions in agreement with the measurement despite the limited complexity of the models: for example, the concentration of oxygen is constant throughout the simulation using the Geant4-DNA toolkit. Despite the variability of measurements and the limitations of simulations, the transient radio-induced hypoxia formulated in the oxygen depletion hypothesis is unlikely to occur. The simulations and most experiments do not consider the re-oxygenation component of the hypothesis. However, the low rates of oxygen depletion do not support the oxygen depletion hypothesis [22] as stated. A more complex alternative, considering biological specificities, should be investigated.

Conclusion

The results obtained in this work are consistent with the literature, supporting the accuracy of Geant4-DNA simulations with scavengers using the continuum approach. As is well known, the radiolysis of pure water is an over-simplified model to study the impact of radiation on biological tissues. The scavenger model, now available in both SBS and IRT methods of Geant4-DNA, makes it possible to overcome this limitation by enabling the addition of any molecule in water, including dissolved oxygen. By introducing specific chemical reactions with their associated rate constant, this model can also simulate cell-relevant scavenging mechanisms. The advantage of Geant4-DNA is the free access to its source code, which allows users to benefit from all developments. Trying to understand the FLASH effect opens up vast unknowns in our comprehension of the effect of radiation on living beings. Modeling using Monte Carlo codes can contribute to this effort, and developments such as improving the complexity of the simulation by adding macromolecules (plasmids, lipids), extending the simulation to the homogeneous chemical stage or including a dose rate are examples of possible directions to follow.

Declaration of Competing Interest

The authors declare that they have no known competing financial interests or personal relationships that could have appeared to influence the work reported in this paper.

Acknowledgements

This work was supported by FNS Synergia grant MAGIC-FNS CRS II5_186369.

Appendix A. Supplementary data

Supplementary data to this article can be found online at https://doi.org/10.1016/j.ejmp.2023.102549.

References

[1] Pimblott SM, LaVerne JA, Mozumder A, Green NJB. Structure of electron tracks in water. 1. Distribution of energy deposition events. J Phys Chem 1990;94(1):488–95. https://doi.org/10.1021/j100364a084.
[2] Pimblott SM, Mozumder A. Structure of electron tracks in water. 2. Distribution of primary ionizations and excitations in water radiolysis. J Phys Chem 1991;95(19):7291–300. https://doi.org/10.1021/j100172a036.
[3] LaVerne JA. Track Effects of Heavy Ions in Liquid Water. Radiat Res 2000;153(5):487–96. https://doi.org/10.1667/0033-7587(2000)153[0487:TEOHII]2.0.CO;2.
[4] Casiraghi M, Bashkirov V, Hurley F, Schulte R. A novel approach to study radiation track structure with nanometer-equivalent resolution. Eur Phys J D 2014;68(5):111. https://doi.org/10.1140/epjd/e2014-40841-0.
[5] Chmielewski AG, Szołucha MM. Radiation chemistry for modern nuclear energy development. Radiat Phys Chem 2016;124:235–40. https://doi.org/10.1016/j.radphyschem.2016.01.002.
[6] O'Neill P, Wardman P. Radiation chemistry comes before radiation biology. Int J Radiat Biol 2009;85(1):9–25. https://doi.org/10.1080/09553000802640401.
[7] Favaudon V, Caplier L, Monceau V, Pouzoulet F, Sayarath M, Fouillade C, et al. Ultrahigh dose-rate FLASH irradiation increases the differential response between normal and tumor tissue in mice. Sci Transl Med 2014;6(245):245ra93.. https://doi.org/10.1126/scitranslmed.3008973.
[8] Incerti S, Baldacchino G, Bernal M, Capra R, Champion C, Francis Z, et al. The geant4-dna project. Int J Model Simul Sci Comput 2010;1(2):157–78. https://doi.org/10.1142/S1793962310000122.
[9] Incerti S, Ivanchenko A, Karamitros M, Mantero A, Moretto P, Tran HN, et al. Comparison of GEANT4 very low energy cross section models with experimental data in water. Med Phys 2010;37(9):4692–708. https://doi.org/10.1118/1.3476457.
[10] Bernal MA, Bordage MC, Brown JMC, Davídková M, Delage E, El Bitar Z, et al. Track structure modeling in liquid water: A review of the Geant4-DNA very low energy extension of the Geant4 Monte Carlo simulation toolkit. Phys Med 2015;31(8):861–74. https://doi.org/10.1016/j.ejmp.2015.10.087.
[11] Incerti S, Kyriakou I, Bernal MA, Bordage MC, Francis Z, Guatelli S, et al. Geant4-DNA example applications for track structure simulations in liquid water: A report from the Geant4-DNA Project. Med Phys 2018;45(8):e722–39. https://doi.org/10.1002/mp.13048.
[12] Draganic IG, Draganic ZD. The Radiation Chemistry of Water. Academic Press; 1971.
[13] Farhataziz R. MAJ. Radiation Chemistry: Principles and Applications. VCH Publishers; 1987.
[14] Plante I, Devroye L. Considerations for the independent reaction times and step-by-step methods for radiation chemistry simulations. Radiat Phys Chem 2017;139:157–72. https://doi.org/10.1016/j.radphyschem.2017.03.021.
[15] Valota A, Ballarini F, Friedland W, Jacob P, Ottolenghi A, Paretzke HG. Modelling study on the protective role of OH radical scavengers and DNA higher-order structures in induction of single- and double-strand break by gamma-radiation. Int J Radiat Biol 2003;79(8):643–53. https://doi.org/10.1080/09553000310001596977.
[16] Boscolo D, Krämer M, Fuss MC, Durante M, Scifoni E. Impact of Target Oxygenation on the Chemical Track Evolution of Ion and Electron Radiation. Int J Mol Sci 2020;21(2):424. https://doi.org/10.3390/ijms21020424.
[17] Sanguanmith S, Meesungnoen J, Stuart CR, Causey P, Jay-Gerin JP. Self-radiolysis of tritiated water. 4. The scavenging effect of azide ions (N3−) on the molecular hydrogen yield in the radiolysis of water by 60Co γ-rays and tritium β-particles at room temperature. RSC Adv 2018;8(5):2449–58. https://doi.org/10.1039/C7RA12397C.

[18] Ramos-Méndez J, LaVerne JA, Domínguez-Kondo N, Milligan J, Štěpán V, Stefanová K, et al. TOPAS-nBio validation for simulating water radiolysis and DNA damage under low-LET irradiation. Phys Med Biol 2021;66(17):175026. https://doi.org/10.1088/1361-6560/ac1f39.
[19] Lai Y, Jia X, Chi Y. Modeling the effect of oxygen on the chemical stage of water radiolysis using GPU-based microscopic Monte Carlo simulations, with an application in FLASH radiotherapy. Phys Med Biol 2021;66(2):025004. https://doi.org/10.1088/1361-6560/abc93b.
[20] Ramos-Méndez J, Shin WG, Karamitros M, Domínguez-Kondo J, Tran NH, Incerti S, et al. Independent reaction times method in Geant4-DNA: Implementation and performance. Med Phys 2020;47(11):5919–30. https://doi.org/10.1002/mp.14490.
[21] Jaccard M, Durán MT, Petersson K, Germond JF, Liger P, Vozenin MC, et al. High dose-per-pulse electron beam dosimetry: Commissioning of the Oriatron eRT6 prototype linear accelerator for preclinical use. Med Phys 2018;45(2):863–74. https://doi.org/10.1002/mp.12713.
[22] Montay-Gruel P, Acharya MM, Petersson K, Alikhani L, Yakkala C, Allen BD, et al. Long-term neurocognitive benefits of FLASH radiotherapy driven by reduced reactive oxygen species. Proc Natl Acad Sci 2019;116(22):10943–51. https://doi.org/10.1073/pnas.1901777116.
[23] Pimblott SM, Pilling MJ, Green NJB. Stochastic models of spur kinetics in water. Int J Radiat Appl Instrum Part C Radiat Phys Chem 1991;37(3):377–88. https://doi.org/10.1016/1359-0197(91)90006-N.
[24] Geant4 Collaboration. Physics Reference Manual. Published online December 2021.
[25] Frongillo Y, Goulet T, Fraser MJ, Cobut V, Patau JP, Jay-Gerin JP. Monte Carlo Simulation of Fast Electron and Proton Tracks in Liquid Water - II. Nonhomogeneous Chemistry Radiat Phys Chem 1998;51(3):245–54. https://doi.org/10.1016/S0969-806X(97)00097-2.
[26] Buxton GV, Greenstock CL, Helman WP, Ross AB. Critical Review of rate constants for reactions of hydrated electrons, hydrogen atoms and hydroxyl radicals (·OH/·O−) in Aqueous Solution. J Phys Chem Ref Data 1988;17(2):513–886. https://doi.org/10.1063/1.555805.
[27] Hata K, Inoue H, Kojima T, Iwase A, Kasahara S, Hanawa S, et al. Hydrogen Peroxide Production by Gamma Radiolysis of Sodium Chloride Solutions Containing a Small Amount of Bromide Ion. Nucl Technol 2016;193(3):434–43. https://doi.org/10.13182/NT15-32.
[28] Agostinelli S, Allison J, Amako K, Apostolakis J, Araujo H, Arce P, et al. Geant4—a simulation toolkit. Nucl Instrum Methods Phys Res A 2003;506(3):250–303. https://doi.org/10.1016/S0168-9002(03)01368-8.
[29] Allison J, Amako K, Apostolakis J, Araujo H, Arce Dubois P, Asai M, et al. Geant4 developments and applications. IEEE Trans Nucl Sci 2006;53(1):270–8. https://doi.org/10.1109/TNS.2006.869826.
[30] Allison J, Amako K, Apostolakis J, Arce P, Asai M, Aso T, et al. Recent developments in Geant4. Nucl Instrum Methods Phys Res A 2016;835:186–225. https://doi.org/10.1016/j.nima.2016.06.125.
[31] Kellerer AM. Considerations on the Random Traversal of Convex Bodies and Solutions for General Cylinders. Radiat Res 1971;47(2):359–76. https://doi.org/10.2307/3573243.
[32] Hartmann GH, Andreo P. Fluence calculation methods in Monte Carlo dosimetry simulations. Z Med Phys 2019;29(3):239–48. https://doi.org/10.1016/j.zemedi.2018.08.003.
[33] Sander R. Compilation of Henry's law constants (version 4.0) for water as solvent. Atmospheric. Chem Phys 2015;15(8):4399–981. https://doi.org/10.5194/acp-15-4399-2015.
[34] Shin WG, Ramos-Mendez J, Faddegon B, Tran HN, Villagrasa C, Perrot Y, et al. Evaluation of the influence of physical and chemical parameters on water radiolysis simulations under MeV electron irradiation using Geant4-DNA. J Appl Phys 2019;126(11):114301. https://doi.org/10.1063/1.5107511.
[35] Draganic ZD, Draganic IG. Studies on the formation of primary yields of hydrogen peroxide and molecular hydrogen (G(H2O2) and G(H2)) in the γ-radiolysis of neutral aqueous solutions. J Phys Chem 1971;75(26):3950–7. https://doi.org/10.1021/j100695a006.
[36] Hiroki A, Pimblott SM, LaVerne JA. Hydrogen Peroxide Production in the Radiolysis of Water with High Radical Scavenger Concentrations. J Phys Chem A 2002;106(40):9352–8. https://doi.org/10.1021/jp0207578.
[37] Pastina B, LaVerne JA. Hydrogen Peroxide Production in the Radiolysis of Water with Heavy Ions. J Phys Chem A 1999;103(11):1592–7. https://doi.org/10.1021/jp984433o.
[38] Štefanić I, LaVerne JA. Temperature Dependence of the Hydrogen Peroxide Production in the γ-Radiolysis of Water. J Phys Chem A 2002;106(2):447–52. https://doi.org/10.1021/jp0131830.
[39] Kyriakou I, Emfietzoglou D, Incerti S. Status and Extension of the Geant4-DNA Dielectric Models for Application to Electron Transport. Front Phys 2022;9:711317. https://doi.org/10.3389/fphy.2021.711317.
[40] Bordage MC, Bordes J, Edel S, Terrissol M, Franceries X, Bardiès M, et al. Implementation of new physics models for low energy electrons in liquid water in Geant4-DNA. Phys Med 2016;32(12):1833–40. https://doi.org/10.1016/j.ejmp.2016.10.006.
[41] Kyriakou I, Šefl M, Nourry V, Incerti S. The impact of new Geant4-DNA cross section models on electron track structure simulations in liquid water. J Appl Phys 2016;119(19):194902. https://doi.org/10.1063/1.4950808.
[42] NIST Standard Reference Database 124. Stopping-Power & Range Tables for Electrons, Protons, and Helium Ions. Accessed May 4, 2022. 10.18434/T4NC7P.
[43] Tran HN, Chappuis F, Incerti S, Bochud F, Desorgher L. Geant4-DNA Modeling of Water Radiolysis beyond the Microsecond: An On-Lattice Stochastic Approach. Int J Mol Sci 2021;22(11):6023. https://doi.org/10.3390/ijms22116023.
[44] Boscolo D, Scifoni E, Durante M, Krämer M, Fuss MC. May oxygen depletion explain the FLASH effect? A chemical track structure analysis. Radiother Oncol 2021;162:68–75. https://doi.org/10.1016/j.radonc.2021.06.031.
[45] Weiss H, Epp ER, Heslin JM, Ling CC, Santomasso A. Oxygen depletion in cells irradiated at ultra-high dose-rates and at conventional dose-rates. Int J Radiat Biol Relat Stud Phys Chem Med 1974;26(1):17–29. https://doi.org/10.1080/09553007414550901.
[46] Jansen J, Knoll J, Beyreuther E, Pawelke J, Skuza R, Hanley R, et al. Does FLASH deplete oxygen? Experimental evaluation for photons, protons, and carbon ions. Med Phys 2021;48(7):3982–90. https://doi.org/10.1002/mp.14917.
[47] Cao X, Zhang R, Esipova TV, Allu SR, Ashraf R, Rahman M, et al. Quantification of Oxygen Depletion During FLASH Irradiation In Vitro and In Vivo. Int J Radiat Oncol Biol Phys 2021;111(1):240–8. https://doi.org/10.1016/j.ijrobp.2021.03.056.
[48] Michaels HB. Oxygen depletion in irradiated aqueous solutions containing electron affinic hypoxic cell radiosensitizers. Int J Radiat Oncol Biol Phys 1986;12(7):1055–8. https://doi.org/10.1016/0360-3016(86)90224-5.
[49] Whillans DW, Rauth AM. An Experimental and Analytical Study of Oxygen Depletion in Stirred Cell Suspensions. Radiat Res 1980;84(1):97–114. https://doi.org/10.2307/3575221.
[50] Palcic B, Skarsgard LD. Reduced Oxygen Enhancement Ratio at Low Doses of Ionizing Radiation. Radiat Res 1984;100(2):328–39. https://doi.org/10.2307/3576354.